Magnetic phases of the triangular Kondo lattice

M. Keßler and R. Eder
Karlsruher Institut für Technologie, Institute for Quantum Materials and Technologies, 76021 Karlsruhe, Germany

(Received 13 October 2020; revised 25 November 2020; accepted 30 November 2020; published 11 December 2020)

The Kondo lattice model (KLM) on the 2-dimensional triangular lattice is studied by bond fermion theory. Three-sublattice Néel order (AF) and partial Kondo screening (PKS) are considered as possible phases of the model. We find that near half filling and at moderate interaction strength, AF and PKS are energetically close and favored compared to the paramagnetic phase. We discuss the quasiparticle band structure and Fermi surface of the different phases. As is the case for the KLM on the square lattice, both the AF and the PKS phase can be further subdivided into phases with the same symmetry, but different Fermi surface topology.

DOI: 10.1103/PhysRevB.102.235125

I. INTRODUCTION

Heavy-fermion compounds have been an active topic of research for the last decades. These systems are characterized by an extraordinarily large effective electron mass, which has been linked to strong electronic correlations in the partially filled $4f$ shells of rare-earth ions or the $5f$ shell of uranium.

Among the many interesting experimental results in heavy-fermion research, a large niche is dedicated to exotic magnetic orderings. Generally, they are caused by two competing effects [1]. On one hand, the RKKY interaction (magnetic correlations between the localized spins mediated through the conduction band) drives the system to magnetic order [2]. On the other hand, through the mechanism known as the Kondo effect, conduction electrons can instead screen the magnetic moments by forming singlet bonds with them [3]. Depending on the strength of the interaction, these singlets may be bound tightly enough so as to leave a gap in the energy spectrum and enable the possibility of a Kondo insulator.

A simple model that captures the main features of this arrangement is the Kondo lattice model (KLM), where each site consists of a conducting c and a localized f orbital that interact antiferromagnetically:

$$H = H_t + H_j, \tag{1}$$

$$H_t = -t \sum_{\langle i,j\rangle,\sigma} c^\dagger_{i\sigma} c_{j\sigma}, \tag{2}$$

$$H_J = J \sum_i \mathbf{S}_c \cdot \mathbf{S}_f, \tag{3}$$

where $c^\dagger_{i,\sigma}$ and $f^\dagger_{i,\sigma}$ create an electron with z spin σ in the respective orbital in unit cell i. Moreover, $\mathbf{S}_{c/f}$ is the spin operator for the c/f electrons, and the angle brackets denote pairs of nearest neighbors. The f orbital is constrained to be occupied by exactly one electron, so that it is equivalent to a spin-1/2 moment. This reflects that the KLM is the strong-coupling limit of the more realistic periodic Anderson model (PAM) [4]. It should be noted that Hamiltonian (1) as it stands implicitly contains the full RKKY interaction and no additional exchange terms between f spins are needed. We consider a system with N unit cells; the number of conduction electrons is N_c, so that the total number of electrons is $N_e = N + N_c$. Densities are denoted by $n_c = N_c/N$ and $n_e = N_e/N$, and t will be used as the unit of energy from here onward.

In the present paper we study this model on a two-dimensional triangular lattice, which brings about the additional complication of geometric frustration. For the KLM one can in fact envisage two different scenarios of how the system resolves the frustration (see Fig. 1). The first one is three-sublattice Néel order, where the magnetic moments on the different sublattices form an angle of 120° with respect to each other. This scenario is known to be realized in the 2d triangular Heisenberg antiferromagnet [5–7]. A second possibility, which is available only to the Kondo lattice, is partial Kondo screening [8–12]. Here, magnetic moments are formed only on a subset of sites, whereas the remaining sites remain nonmagnetic. For example, if one third of the sites in the triangular lattice remain nonmagnetic, the remaining sites can form a honeycomb lattice which allows for standard two-sublattice Néel order. In fact, for some geometrically frustrated-heavy fermion compounds (such as UNi_4B [13–15], CePdAl [16,17], or $Ce_5Ni_2Si_3$ [18]) experiments indicate that part of the Ce or U ions remain paramagnetic even in magnetically ordered phases, consistent with the notion of partial Kondo screening.

A large number of mean-field studies [19–29] and numerical calculations [30–44] have been devoted to the study of the Kondo lattice and its possible ordering transitions. For the two-dimensional square lattice in particular, numerical studies such as quantum Monte Carlo (QMC) [35], variational Monte Carlo (VMC) [38–40], the dynamical mean-field approximation (DMFT) [43], and bond fermion theory [45,46] give a relatively consistent picture: for the case of the Kondo insulator (conduction electron density $n_c = 1$) the KLM has a paramagnetic ground state for $J/t > J_c/t \approx 1.4$. With decreasing J/t there is a 2nd-order phase transition at J_c/t and Néel order sets in [35,45]. Upon hole doping, $n_c < 1$ (i.e., going over to metallic systems), the 2nd-order transition is

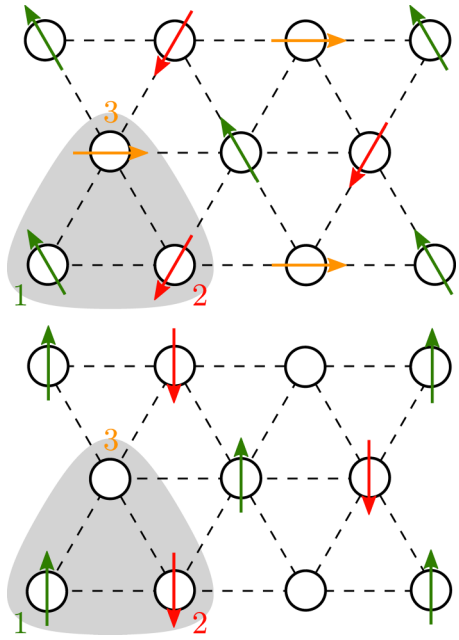

FIG. 1. Schematic view of the net magnetic moments in the 120° Néel (top) and partial Kondo screening (bottom) phases. The colored numbers indicate the sublattice index; atoms with same-colored arrows belong to the same sublattice. The atoms underlaid in gray form a single unit cell of the ordered system. Note that sublattice 3 does not carry a net magnetic moment in the partial Kondo screening phase.

rapidly shifted to smaller J/t and a 1st-order transition between two metallic antiferromagnetic phases with different Fermi surface topology occurs [38–40,43,46]. For the KLM or PAM on the 2d triangular lattice, on the other hand, fewer results are available and the situation is less clear [50–58].

The qualitative behavior of the KLM on the 2d square lattice has been reproduced by bond fermion theory [46,47]. Encouraged by this, we apply this formalism to explore the phase diagram of the triangular lattice, whereby we consider three-sublattice antiferromagnetism and partial Kondo screening.

II. BOND FERMION THEORY

The model is solved using a generalization of the bond fermion theory [46,47]. Let us consider the limit $t/J \ll 1$ and a conduction electron density $n_c = 1$. In this case hopping between different sites will be suppressed. Consequently, the wave function of the system can be approximately described as a product of single-site wave functions, with each site occupied by exactly two electrons. The most general such state is given by

$$|\Omega\rangle = \prod_j^N g_j^\dagger |0\rangle\,, \tag{4}$$

$$g_j^\dagger = (u_j^* s_j^\dagger + \mathbf{v}_j^* \cdot \mathbf{t}_j^\dagger); \tag{5}$$

$s_j^\dagger$ and $\mathbf{t}_j^\dagger$ generate singlet and triplet configurations on site j, respectively. In four-vector notation and introducing the vector of Pauli matrices $*\tau$, they can be written as

$$(s_j^\dagger,\ \mathbf{t}_j^\dagger) = \frac{1}{\sqrt{2}} \sum_{\sigma,\sigma'} c_{j\sigma}^\dagger (i\tau_y,\ *\tau\, i\tau_y)_{\sigma,\sigma'} f_{j\sigma'}^\dagger. \tag{6}$$

u and $\mathbf{v}$ are (in general complex) coefficients. Normalization of $|\Omega\rangle$ requires

$$|u_j|^2 + |\mathbf{v}_j|^2 = 1. \tag{7}$$

Unlike in previous works [46,47] we must also consider configurations with $\mathbf{v}_j$ not parallel to the z axis to properly describe the planar 120° antiferromagnetic order.

The expectation value of H in the state $|\Omega\rangle$ is

$$E_\Omega = -\sum_j e_j, \tag{8}$$

$$e_j = J\left(\frac{3}{4}|u_j|^2 - \frac{1}{4}|\mathbf{v}_j|^2\right). \tag{9}$$

As is to be expected, in the absence of hopping, the ground state will be paramagnetic ($\mathbf{v}_j = 0$). At finite t, the system will experience charge fluctuations, where electrons are transferred from one site to another. This results in sites occupied by one or three electrons, which can propagate through the lattice by further hopping processes. As a result of this mechanism, a nonvanishing $\mathbf{v}_j$ may be energetically favorable.

We describe the charge fluctuations as fermionic particles a and b (referred to as "bond fermions") and define the following mapping between states of the true Kondo lattice and states of the bond fermions [47]:

$$\prod_{j\in S_a} f_{j,\sigma(j)}^\dagger \prod_{j\in S_b} c_{j,\uparrow}^\dagger c_{j,\downarrow}^\dagger f_{j,\sigma(j)}^\dagger \prod_{j\in\overline{(S_a\cup S_b)}} g_j^\dagger |0\rangle \equiv \prod_{j\in S_a} a_{j,\sigma(j)}^\dagger \prod_{j\in S_b} b_{j,\sigma(j)}^\dagger |\mathrm{vac}\rangle\,. \tag{10}$$

Thereby $|\mathrm{vac}\rangle$ is the vacuum state of the bond particles, equivalent to $|\Omega\rangle$. Here $\sigma(j)$ is an arbitrary function of the site index and as can be seen above, $a_{j,\sigma}^\dagger$ ($b_{j,\sigma}^\dagger$) stands for a configuration with zero (two) conduction electrons on site j. The sites in S_a (S_b) thus are occupied by hole-like (electron-like) particles, whereas the remainder of sites, $\overline{(S_a \cup S_b)}$, is "filled" with mixed singlet-triplet states. The sets S_a and S_b obviously must be disjoint for this mapping to make sense (a "hard-core" constraint, meaning that every site can only be occupied by at most a single bond fermion). Since exchanging any factors in the first two products of the left-hand site creates a minus sign, the bond particles must in fact be fermions. Equation (10) also highlights the key advantage of the bond fermion calculation: all states on the left-hand side obey the constraint to have precisely one f electron per site exactly. Bond fermion theory thus trades the constraint on the f electrons (which

form a dense system) for the hard-core constraint on the bond fermions, which form a dilute system in many situations of interest (see below).

We will now rewrite the Hamiltonian in terms of bond fermions, by demanding that the matrix elements of the bond fermion Hamiltonian between the states on the right-hand side are equal to those of the true Kondo lattice between the states on the left-hand side. This representation cannot be completely faithful, as we have disregarded purely spin excitations (where a site is occupied by two electrons, but in a different spin state than $|\Omega\rangle$). This corresponds to a truncation of our Hilbert space.

The exchange energy of a site with zero or two conduction electrons vanishes, so we ascribe an energy of e_j to the creation of a bond fermion out of $|\Omega\rangle$:

$$H_J \equiv \tilde{H}_J = E_\Omega + \sum_{j,\sigma} e_j (a^\dagger_{j,\sigma} a_{j,\sigma} + b^\dagger_{j,\sigma} b_{j,\sigma}). \tag{11}$$

The kinetic part of the Hamiltonian is constructed by translating the conduction electron operators into bond fermions. Collecting the different species into a four-component vector

$$z_j = (a^\dagger_{j,\uparrow} \;\; a^\dagger_{j,\downarrow} \;\; b_{j,\uparrow} \;\; b_{j,\downarrow})^\intercal, \tag{12}$$

the representation reads [48]

$$\begin{aligned} c_{j,\sigma} &\equiv \tilde{c}_{j,\sigma} = (W_j)_{\sigma\alpha}(z_j)_\alpha, \\ W_j &= \frac{1}{\sqrt{2}}([u_j + \mathbf{v}_j \cdot *\tau] i\tau_y \quad [-u_j^* + \mathbf{v}_j^* \cdot *\tau]) \end{aligned} \tag{13}$$

with the 2×4-matrix W_j. In this way the hopping terms becomes

$$H_t \equiv \tilde{H}_t = -t \sum_{\langle i,j \rangle} z_i^\dagger W_i^\dagger W_j z_j. \tag{14}$$

The total number of electrons (including both conduction and localized bands) can be calculated by noting that the state $|\Omega\rangle$ has two electrons per unit cell and each a (b) fermion decreases (increases) this by 1:

$$N_e = 2N + \sum_{j,\sigma} (b^\dagger_{j,\sigma} b_{j,\sigma} - a^\dagger_{j,\sigma} a_{j,\sigma}) \tag{15}$$

$$= \sum_{j,\sigma} (a_{j,\sigma} a^\dagger_{j,\sigma} + b^\dagger_{j,\sigma} b_{j,\sigma}) = \sum_j z_j^\dagger z_j. \tag{16}$$

Alternatively, we can substitute the Fourier transform of (13) into $\langle c^\dagger_{\boldsymbol{k},\sigma} c_{\boldsymbol{k},\sigma} \rangle$ and sum over $\boldsymbol{k}$ and σ to obtain N_c, the number of conduction electrons. Numerical evaluation shows that these two ways of calculating N_c do not give consistent results. This is a consequence of the truncation of the Hilbert space: part of the spectral weight of the electron operators has been lost. We follow Ref. [46] and enforce the equivalence of both expressions through a Lagrange multiplier λ. This was shown to lead to "heavy" bands pinned near the Fermi energy of the unhybridized conduction bands [49], which is the correct physical picture. In addition we relax the hard-core constraint on the bond fermions. This is reasonably justified as long as the density of bond fermions is low, which is fulfilled [46] for at least moderately large J/t and electron densities close to half filling. The system can now be solved as a free fermion gas by diagonalizing the Hamiltonian in momentum space. Note that $\tilde{H}_t$ contains terms $\propto a^\dagger_{i,\sigma} b^\dagger_{j,\sigma'}$, so that the excitations of the system are Bogoliubov particles.

We have mentioned that the bond fermion theory implies a truncation of the Hilbert space and necessitates the relaxation of the hard-core constraint. Still, the previous success of the bond fermion theory in reproducing the qualitatively correct phase diagram and band structure of the square Kondo lattice [46] gives us some confidence that these approximations are justified also for the much less well studied triangular lattice. However, two deficiencies of the bond fermion theory that were uncovered during this study should be kept in mind.

First, it appears that bond fermion theory overestimates the tendency toward magnetic ordering: for the square lattice at $n_c = 1$ (the Kondo insulator) bond fermion theory predicts the critical interaction strength for the onset of antiferromagnetic order as $J_c/t = 2.2$ [46], whereas the exact value is $J_c/t = 1.45$ [35]. On the other hand, the correct value of J_c/t is difficult to obtain even for numerical methods: VMC finds $J_c/t = 1.7$ [38], DMFT finds $J_c/t = 2.2$ [43], and the dynamical cluster approximation finds $J_c/t = 2.1$ [42]. However, the phase diagram and the band structure's behavior as a function of J are reproduced quite well when J is instead measured in units of J_c [46,47]. We thus expect that the overall scale of the phase diagram for the triangular lattice will also be somewhat off.

Second, we stress that the bond fermion theory cannot reproduce the energy scale of the Kondo temperature $\propto e^{-\frac{1}{\rho J}}$, expected to be relevant for $J/t \ll 1$. This should not be a major limitation as we are mostly interested in the emergence of magnetic order. For the square lattice, previous experience shows [35,38,42,43] that magnetic transitions appear mostly for $J/t > 1$, and this seems reasonable for the triangular lattice as well (our results will support this). These magnetic phases are stabilized through the RKKY interaction implicit in the KLM of (1), which express themselves in the bond fermion method as part of the kinetic energy (14). As $W_i^\dagger$ and W_j respectively depend on $\mathbf{v}_i$ and $\mathbf{v}_j$, the hopping terms are influenced by the strengths and relative orientations of both magnetic moments.

III. CALCULATION

In addition to the paramagnetic state with $\mathbf{v}_j = 0$, we consider three different kinds of magnetic ordering (see again Fig. 1): ferromagnetic (F), 120° antiferromagnetic (AF), and partially Kondo screened (PKS). The latter two break the translational symmetry of the model and are implemented on an enlarged, 3-site unit cell. The AF phase is a planar, noncollinear ordering, and corresponds to the minimum-energy configuration of classical, fixed-length spins. In the PKS phase, only two of the three sites carry a net magnetic moment. This effectively turns the sublattice of magnetically ordered sites into a (nonfrustrated) honeycomb lattice.

We take u_j and $\mathbf{v}_j$ to be real and homogeneous on each of the three sublattices. Explicitly, we set ($I = 1, 2, 3$ is the sublattice index)

$$\text{F}: \quad u_I = \cos(\Theta), \tag{17}$$

$$\mathbf{v}_I = \sin(\Theta)\hat{e}_z, \tag{18}$$

$$\text{AF}: \quad u_I = \cos(\Theta), \tag{19}$$

$$\mathbf{v}_I = \sin(\Theta)\left[\hat{e}_x \cos\left(\frac{2\pi}{3} I\right) + \hat{e}_y \sin\left(\frac{2\pi}{3} I\right)\right], \tag{20}$$

$$\text{PKS}: \quad u_1 = u_2 = \cos(\Theta), \qquad u_3 = 1, \tag{21}$$

$$\mathbf{v}_1 = -\mathbf{v}_2 = \sin(\Theta)\hat{e}_z, \qquad \mathbf{v}_3 = 0; \tag{22}$$

Θ controls the degree of triplet (magnetic) admixture in $|\Omega\rangle$. Paramagnetism corresponds to $\Theta = 0$. For sites which carry a magnetic moment the exchange energy is given by $e_j = e(\Theta) = J/4[1 + 2\cos(2\Theta)]$.

The phase diagram is found by minimizing the Helmholtz free energy over the range $0 \leqslant \Theta \leqslant \pi/3 = 1.05$ for each type of magnetic order.

Our approximations become inapplicable for $\pi/3 < \Theta$ because the bond fermions' energy of formation $e(\Theta)$ becomes negative in this region. Consequently, it is energetically favorable to create as many bond fermions as possible and due to the presence of pair creation terms $\propto a^\dagger_{i,\sigma} b^\dagger_{j,\sigma'}$ the system is filled with fermions. In fact, the ground states in this region of $\Theta > \pi/3$ have bond fermion densities of 2 to 3 per site, which is entirely unphysical in view of the hard-core constraint. In contrast, our solutions will have densities less than 0.8 (and decreasing with J), with the probability for a constraint violation always below 20%.

We can already address one significant difference between the AF and PKS phase, namely the different band degeneracy. For the PKS phase spatial parity inversion ($\mathcal{P}$) about a nonmagnetic lattice site exchanges the two magnetic sublattices (compare Fig. 1, bottom). The original state of the lattice can then be restored by flipping the magnetic moments through a time reversal ($\mathcal{T}$), so that a $\mathcal{PT}$ operation is a remaining (antiunitary) symmetry of the ordered system. When acting with $\mathcal{PT}$ on a Bloch state $\propto e^{i\mathbf{kr}}$, each of $\mathcal{P}$ and $\mathcal{T}$ involves exchanging $\mathbf{k} \to -\mathbf{k}$, so that the crystal momentum remains unchanged. However, $\mathcal{T}$ does not commute with S_z, the bond fermion spin in the z direction, which is conserved as the system is spin rotation invariant about the z axis. Accordingly, for every $\mathbf{k}$, we must have degenerate states that can be distinguished by their spin direction; see Fig. 5. In contrast, $\mathcal{P}$ is not a symmetry operation for the AF phases (see Fig. 1) and the bands in these phases are nondegenerate.

As a final note, we performed all calculations at a small positive temperature $T = 0.0025t$ to avoid numerical problems arising from the zero-temperature Fermi function. We have verified that changing the temperature in this range does not have a noticeable influence on the phase diagram or band structure. We have also checked that the results are converged with respect to the density of $\mathbf{k}$ points in the Brillouin zone.

IV. RESULTS

A. 120° antiferromagnetic phases

For the sake of clarity we first present the results with only AF order taken into account. We find four qualitatively different phases, depicted in Fig. 2. For example, if we were to reduce the ratio J/t starting from large values, with a constant $n_c > 1$, we would first encounter a 2nd-order transition from the paramagnetic phase to the ordered AFI phase (with finite Θ), followed by two successive 1st-order transitions to the AFII and AFIII phases, respectively. While the symmetry of all three ordered phases is the same, they are distinguished by their band structures and Fermi surfaces (Fig. 3).

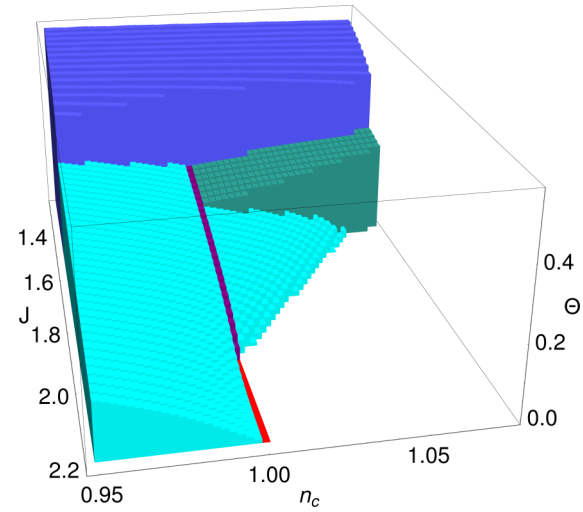

FIG. 2. Optimal mixing angle Θ when considering only AF order. Colors indicate different phases: paramagnetic metal (white) and insulator (red), AFI metal (cyan) and insulator (purple), AFII (turquoise), AFIII (dark blue).

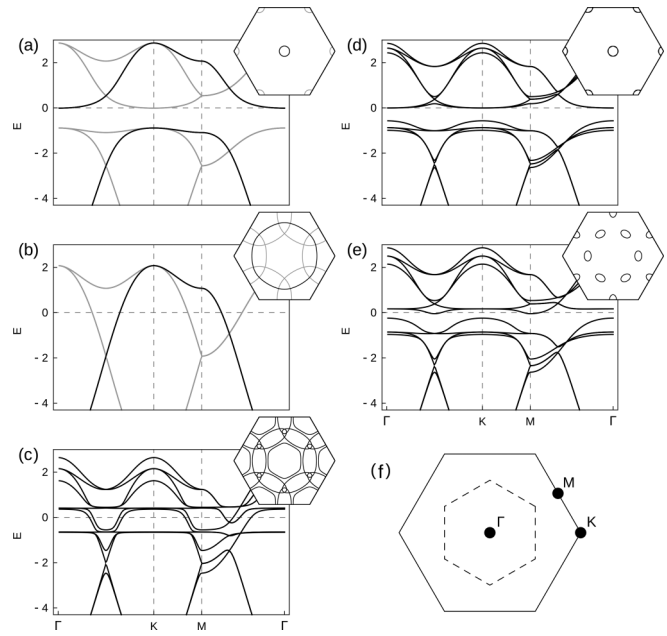

FIG. 3. Band structure of the AF phases on a path through the symmetry points of the large BZ. Energies are given relative to the Fermi energy and $n_c = 1.025$. (a) $J = 1.83t$ P, (b) $J = 0$ noninteracting system (the f band is not shown; it is perfectly flat with $E = 0$), (c) $J = 1.25t$ AFIII, (d) $J = 1.63t$ AFI, (e) $J = 1.51t$ AFII, (f) full (dashed) lines: large (small) BZ and the relevant symmetry points. The hexagonal insets in (a)–(e) show the Fermi surface. (a) and (b) depict irreducible bands in black; antiferromagnetic foldings are shown in gray to help comparison with the other graphs. Note the relative similarity in the positions of Fermi pockets between (a) /(d) and (b) /(c) /(e), respectively.

AFI and AFII have $\Theta < 0.35$ and are analogous to the antiferromagnetic phases found for the square lattice by Watanabe *et al.* [38] using VMC, Peters and Kawakami [43] using DMFT, and through bond fermion theory [46]. The AFI Fermi surface is almost the same as what would be found by a paramagnetic calculation, consisting of a pocket at the Γ point (more precisely, two slightly acircular pockets rotated 60° relative to each other), and its umklapp copies around the BZ edges. These pockets are formed from the flat bands of the f electrons (3) which have become itinerant. This is different in the AFII phase. Here, the Fermi surface is derived from the noninteracting one and the c electrons are the relevant charge carriers.

The quasiparticle band structures in both AFI and AFII are gapped. Approaching half filling from above, the jump in Θ at the AFI-AFII transition vanishes continuously, so that no transition between them occurs for $n_c \leqslant 1$. The reason is that the difference in behavior of AFI and AFII is caused by a slight shift of the minima of the lowest band above the gap (from Γ and K for AFI to M and halfway between Γ and K for AFII) whereas the topmost band below the gap has the same appearance in both cases. This means that below half filling, when the Fermi surface cuts into the band below the gap, the phases coalesce.

AFIII covers the region of $J/t \lesssim 1.45$ and all electron densities considered. The optimal angle is large, $\Theta \sim 0.5$. As a consequence of this, the hybridization between localized and itinerant bands is rather weak: the determinants of the two 2×2 matrices from which the 2×4 matrix W_j in (13) is composed are $u_j^2 - \mathbf{v}_j^2$ and its complex conjugate, respectively. These matrices become singular for $\Theta = \pi/4 = 0.79$, at which point one is left with two effectively independent systems: one set of bands that mimics the band structure of a mean-field calculation, where the interaction with the localized spins is replaced by a sublattice-dependent Zeeman term, and one set of perfectly flat bands above and below the Fermi surface separated by an energy of e_j. The AFIII phase is close enough to this special case that the residual hybridization can be ignored for a qualitative description of the dynamics near the Fermi energy (Fig. 3): the Fermi surface is the result of folding the noninteracting electron bands to the antiferromagnetic Brillouin zone (AFBZ) and hybridizing them. Accordingly, this phase remains conducting even at half filling, in contrast to the other magnetic phases.

For $n_c = 1$, the Fermi energy is located inside the gap and the system becomes insulating. Our calculation predicts a critical value of $J/t = 1.96$ for the formation of magnetic moments, and $J/t = 1.45$ for the transition to the metallic AFIII phase. In the case of $n_c < 1$, Θ vanishes much more slowly and magnetic order survives to larger J/t: the "combined" AFI/AFII phase (which we refer to as AFI because its Fermi surface is the same as the AFI phase at $n_c > 1$) extends up to $J/t \sim 4$ (not pictured).

B. Partial Kondo screening

We now repeat the above calculation, but for PKS-type order. Phases of this type may be favored over AF order in easy-axis anisotropic systems, where noncollinear order is suppressed. On the other hand, since the PKS phase's sublattices cannot all be related by symmetry transformations, this could lead to a charge disproportionation and a higher Coulomb energy that is unaccounted for in our model. As was the case for the AF phase, we find three different ordered phases (Fig. 4), PKSI–III, which are reached for $n_c > 1$ by lowering J. Somewhat surprisingly, the critical value of the interaction at half filling is unchanged at $J/t = 1.96$.

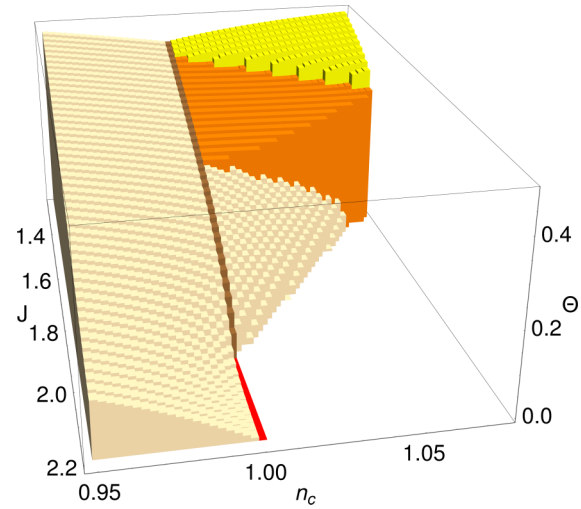

FIG. 4. Same as Fig. 2, but for PKS order: paramagnetic metal (white) and insulator (red), PKSI metal (peach) and insulator (brown), PKSII (orange), PKSIII (yellow).

To begin with, PKSI and PKSII are qualitatively very similar to AFI and AFII, respectively (see Fig. 5). Fermi pockets are found in the same spots as before. Note the relative decrease in area of the Fermi pockets between AFII and PKSII, which is a consequence of the absence of spin degeneracy in the AF phases: since for PKSII each band in a pocket can accommodate two electrons instead of one, their sizes must be halved for the total fermion number to stay the same. This is not the case for AFI and PKSI because (as mentioned earlier) the pocket for AFI actually consists of two slightly different and rotated pockets.

PKSIII does not have an AF analog. Unlike AFIII, the band structure is gapped and becomes insulating when approaching $n_c = 1$. In fact, it is most similar to AFII and PKSII: While the Fermi surfaces of these phases consist of pockets along the *edges* of the small BZ [Fig. 3(f)], they are now placed at the *corners*. The bands below the gap are still unaffected, so that no transition between PKS phases is found at all for $n_c < 1$ and PKSI extends to lower J/t.

Figure 6 summarizes some physical properties along the line of constant $n_c = 1$, namely the angle Θ in (22), the charge disproportionation $n_3 - n_c$ between magnetic and nonmagnetic sites in the PKS phase, and the probabilities p_I for violation of the hard-core constraint on sublattice I. The critical values are $J/t = 1.96$ for P to PKSI and $J/t = 1.38$ for PKSI to AFIII (see Sec. IV C). Note that $\Theta = 0$ for the paramagnetic phase and $n_3 - n_c \neq 0$ only for the PKS phase, whereas $p_3 = p_{1,2}$ for the paramagnetic and AFIII phases. Θ shows square-root behavior directly below the PKS transition, while $n_3 - n_c$ is linear. In addition, $p_I < 0.16$ in the whole range of the plot. In the PKS phase there is a sizable

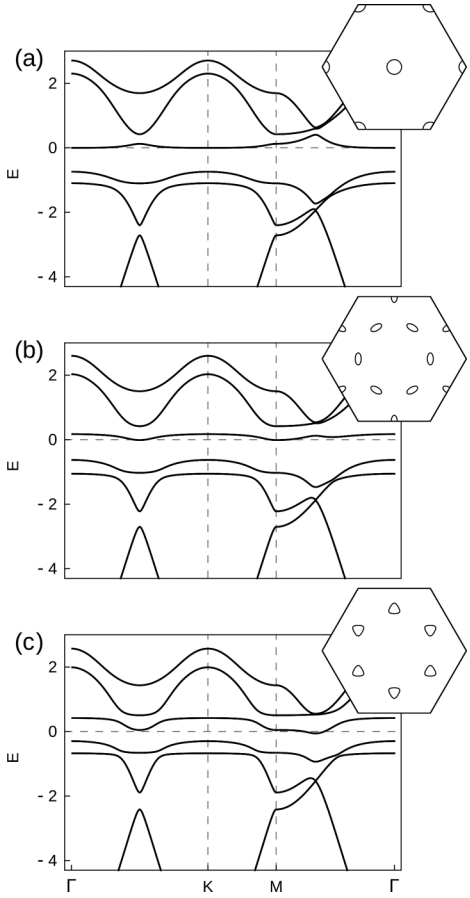

FIG. 5. Same as Fig. 3, but for the PKS phases. (a) $J = 1.63t$ PKSI, (b) $J = 1.51t$ PKSII, (c) $J = 1.25t$ PKSIII.

charge disproportionation $n_3 - n_c$: n_3, the electron density on the third (nonmagnetic) sublattice is found to be significantly higher (in excess of 10% for some parameter regions) than on the other (magnetic) sublattices. On-site Coulomb repulsion will thus be a significant obstacle to PKS phases in more realistic systems.

C. Full phase diagram

We now consider all phases simultaneously, resulting in the combined phase diagram in Figs. 7 and 8. A large part of the PKS region is replaced by AF phases: in particular, PKSIII is completely covered by AFIII. However, PKS is still found in a kite-shaped region around the (insulating) line of $n_c = 1$ and $1.37 < J/t < 1.96$ and a disconnected region for $n_c < 1$ and $J/t \approx 3.2$.

The P metal is replaced by a weakly ferromagnetic phase up to $J/t \sim 5$. The magnetic moment is comparatively small, with the angle $\Theta < 0.05$. The band structure of the F phase (Fig. 9) is very similar to P, but the magnetization results in a spin splitting large enough to completely polarize the Fermi pockets. Accordingly, the area of each Fermi pocket must be doubled. The order parameter vanishes continuously when approaching half filling, so that no insulating ferromagnetic phase is observed.

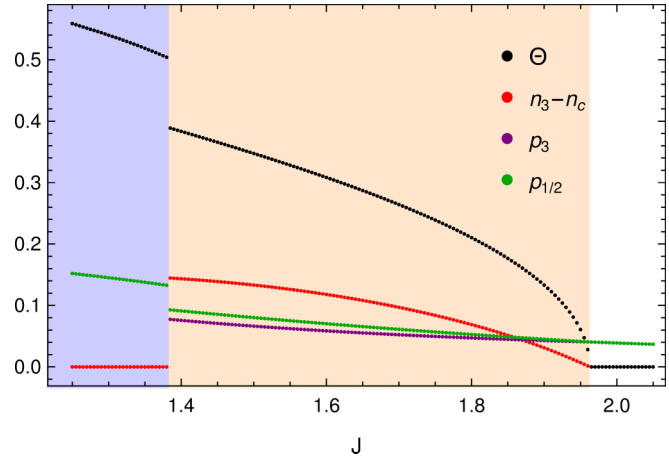

FIG. 6. Details of the system at half filling. Pictured are the order parameter (Θ), the excess electron density on sublattice 3 at half filling ($n_3 - n_c$), and the probability for a constraint violation on the different sublattices (p_3 and $p_{1/2}$). The background color indicates the phase of the system: AFIII metal (blue), PKSI insulator (orange), P insulator (white); compare Fig. 7.

D. Summary and discussion

In summary we have studied the phase diagram of the Kondo lattice model on a two-dimensional triangular lattice, which brings about the additional complication of geometrical frustration. We investigated two ways for the ordered moment to circumvent the frustration, three-sublattice Néel order which is realized in Heisenberg antiferromagnets, and partial Kondo screening where magnetic moments are formed only on a subset of sites which form a honeycomb lattice. Our calculations indicate that both types of magnetic order become stable for smaller J/t and that they are in fact energetically very close to each other. For example, at half filling the critical value of J_c/t where magnetic order sets

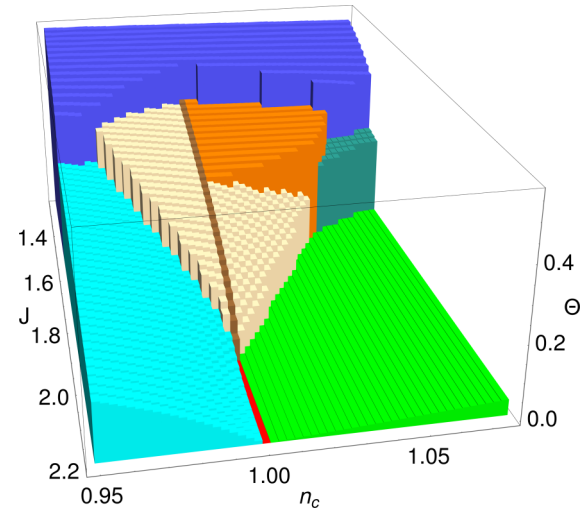

FIG. 7. Same as Figs. 2 and 4, but with all kinds of magnetic order included. Phases appearing are as follows: paramagnetic insulator (red), AFI metal (cyan), AFII (turquoise), AFIII (dark blue), PKSI metal (peach) and insulator (brown), PKSII (orange), F (green).

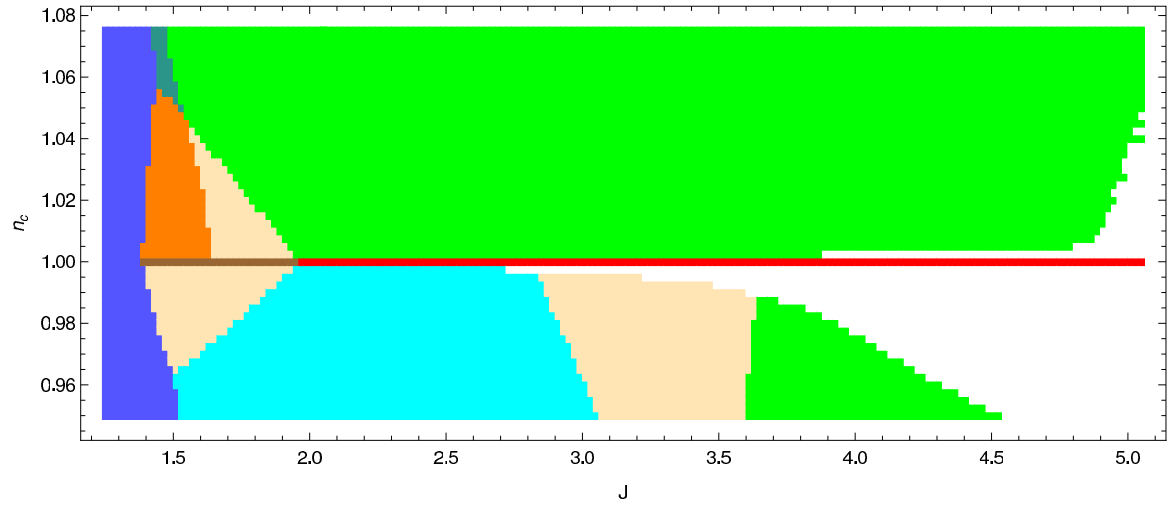

FIG. 8. Extended vertical view of Fig. 7.

in is practically the same for AF and PKS. As was the case for the two-dimensional square lattice, the antiferromagnetic phases themselves actually consist of several phases which differ in their Fermi surface topology. For larger $J/t < J_c/t$ and for both types of magnetic order the band structure and Fermi surface may be obtained by backfolding the paramagnetic band structure, so that one has Fermi pockets formed by the heavy part of the paramagnetic band. Accordingly, the phase transition from paramagnetic to antiferromagnetic is of second order. Upon further reducing J/t there is a 1st-order transition to a phase whose band structure and Fermi surface are consistent with that of the mere conduction band under the influence of decoupled magnetic moments.

We will now try to relate our results to previous works on PKS in the triangular lattice KLM. While some studies have focused on chiral-type magnetic order and treated the localized moments classically [50–52], Motome *et al.* investigated PKS at half filling using VMC [53]. In contrast to our calculation, they do not find any indication that a PKS state exists for $n_c = 1$, unless it is stabilized by an Ising-like interaction between the localized moments. While VMC should in principle yield more accurate results than the somewhat hand-waving approach of the bond fermion theory, one has to keep in mind that the precision of VMC is limited by its restriction to considerably smaller finite systems. The energy differences we find between the different phases are typically very small (the bond fermion theory predicts a maximum relative difference of 2% across the whole parameter region under consideration), while Motome *et al.* estimate a relative accuracy of 3% for their calculation. Here it should be noted that the VMC calculations of Watanabe and Ogata for the square lattice indicate that such small energy differences between paramagnetic and antiferromagnetic phases indeed seem to be typical for the KLM [38]. In that sense the VMC results may not *a priori* invalidate the results of the present paper.

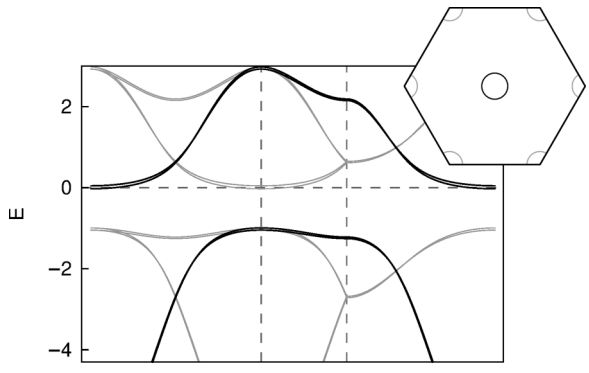

FIG. 9. Same as Figs. 3 and 5, but for the F phase ($J = 2.01t$). Note the slight band splitting.

PKS has also been investigated in the context of the PAM on a triangular lattice, which maps to the KLM in the strong-coupling limit [4]. More precisely, for the symmetric PAM the exchange coupling of the KLM is $J \sim 8V^2/U$, where V is the conduction-band–f-level hybridization and U the Coulomb repulsion on the f level of the PAM. Hayami *et al.* [54,55], have studied the PAM in mean-field approximation and found a phase diagram qualitatively similar to ours for $U = 2t$ [55]. Keeping in mind that we restrict ourselves to homogeneous phases and are thus unable to reproduce the phase-separated regions discussed by Hayami *et al.*, both calculations predict the same phases at half filling: paramagnetic Kondo insulator for large J, antiferromagnetic metal for small J, and PKS in an intermediate region. Additionally, their phase diagram shows a similar tendency toward AF (F) order below (above) half filling. However, the numerical values of J/t at the phase transitions are considerably higher, ranging from 3 to 6. At larger U, the PKS phase is replaced first by a collinear "up-up-down" (UUD) antiferromagnetic phase and then by an insulating 120° AF state [54]. While we did not investigate UUD order, an insulating AF phase at intermediate coupling qualitatively matches our results with PKS disregarded.

Aulbach *et al.* [56] considered the same problem using DMFT. These authors took into account UUD, PKS, and ferromagnetic phases whereas antiferromagnetic 120° order was disregarded. They found magnetic order at less than half-filling (corresponding to $n_c > 1$ as they chose the opposite

sign for the kinetic energy). There, ordered phases are found in two disconnected parameter regions, one with PKS that gives way to UUD order upon lowering J, and, at even further reduced electron densities, one displaying ferromagnetism. In particular, no PKS insulator is found. We have so far been unable to explain this stark contrast to our results (where magnetically ordered phases are favored compared to paramagnetism in much larger regions of parameter space).

Additionally, there is theoretical evidence for PKS at other commensurate fillings [57,58]. We cannot expect our approximations to give sensible results so far away from half filling. For example, Noda *et al.* predict a PKS state and a metal-insulator transition for $n_c = 2/3$, which in our formulation of the bond fermion theory would consists of a state with 5 filled bands. However, the band degeneracy in the PKS makes such a transition impossible, as insulating phases can only exist for an even number of filled bands. To investigate such commensurate fillings, one would have to "switch the vacuum" and choose the ground state $|\Omega\rangle$ and the excitations corresponding to the bond particles such that they already include entanglement between different sites of an enlarged unit cell.

A somewhat puzzling results of the present calculation is the appearance of a weakly ferromagnetic phase which occupies substantial parts of the phase diagram, in particular close to $n_c = 1$. For the 1-dimensional Kondo lattice it can be shown [59] that ferromagnetism occurs for large J/t and any electron density other than $n_c = 1$, whereby the ferromagnetic polarization always takes its maximum value compatible with the electron density. Our ferromagnetic phase would comply with this in that there is complete spin polarization of the Fermi surface. Due to the heavy bands already a very minor admixture of triplets—i.e., a very small Θ—is sufficient to split the bands sufficiently so as to induce complete ferromagnetic polarization. A weakly ferromagnetically polarized Kondo-screened phase has been discussed by various authors [60–62] although usually for electron densities n_c significantly smaller than 1. Moreover a number of ferromagnetic heavy-fermion compounds, often with considerably reduced ordered moment, are known experimentally [63–66].

ACKNOWLEDGMENTS

This work was supported by the Virtual Materials Design initiative within the Helmholtz program Science and Technology of Nanosystems at the Karlsruhe Institute of Technology. The authors acknowledge support by the state of Baden-Württemberg through bwHPC.

[1] S. Doniach, Physica B **91**, 231 (1977).
[2] M. A. Ruderman and C. Kittel, Phys. Rev. **96**, 99 (1954); T. Kasuya, Prog. Theor. Phys. **16**, 45 (1956); K. Yosida, Phys. Rev. **106**, 893 (1957).
[3] J. Kondo, Prog. Theor. Phys. **32**, 37 (1964); K. G. Wilson, Rev. Mod. Phys. **47**, 773 (1975).
[4] J. R. Schrieffer and P. A. Wolff, Phys. Rev. **149**, 491 (1966).
[5] B. Bernu, C. Lhuillier, and L. Pierre, Phys. Rev. Lett. **69**, 2590 (1992).
[6] B. Bernu, P. Lecheminant, C. Lhuillier, and L. Pierre, Phys. Rev. B **50**, 10048 (1994).
[7] L. Capriotti, A. E. Trumper, and S. Sorella, Phys. Rev. Lett. **82**, 3899 (1999).
[8] C. Lacroix, B. Canals, and M. D. Nunez-Regueiro, Phys. Rev. Lett. **77**, 5126 (1996).
[9] M. D. Nunez-Regueiro, C. Lacroix, and B. Canals, Physica C **282-287**, 1885 (1997).
[10] R. Ballou, J. Alloys Compd. **275-277**, 510 (1998).
[11] A. S. Wills, R. Ballou, and C. Lacroix, Phys. Rev. B **66**, 144407 (2002).
[12] C. Lacroix, J. Phys. Soc. Jpn. **79**, 011008 (2010).
[13] S. A. M. Mentink, A. Drost, G. J. Nieuwenhuys, E. Frikkee, A. A. Menovsky, and J. A. Mydosh, Phys. Rev. Lett. **73**, 1031 (1994).
[14] A. Oyamada, M. Kondo, K. Fukuoka, T. Itou, S. Maegawa, D. X. Li, and Y. Haga, J. Phys.: Condens. Matter **19**, 145246 (2007).
[15] R. Movshovich, M. Jaime, S. Mentink, A. A. Menovsky, and J. A. Mydosh, Phys. Rev. Lett. **83**, 2065 (1999).
[16] K. Kamioka, A. Oyamada, K. Hashi, S. Maegawa, T. Goto, H. Kitazawa, and Y. Isikawa, Phys. B: Condens. Matter **259-261**, 121 (1999).
[17] S. Lucas, K. Grube, C.-L. Huang, A. Sakai, S. Wunderlich, E. L. Green, J. Wosnitza, V. Fritsch, P. Gegenwart, O. Stockert, and H. v. Löhneysen, Phys. Rev. Lett. **118**, 107204 (2017).
[18] B. K. Lee, D. H. Ryu, D. Y. Kim, J. B. Hong, M. H. Jung, H. Kitazawa, O. Suzuki, S. Kimura, and Y. S. Kwon, Phys. Rev. B **70**, 224409 (2004).
[19] A. Yoshimori and A. Sakurai, Prog. Theor. Phys. Suppl. **46**, 162 (1970).
[20] C. Lacroix and M. Cyrot, Phys. Rev. B **20**, 1969 (1979).
[21] C. Lacroix, J. Magn. Magn. Mater. **100**, 90 (1991).
[22] A. Auerbach and K. Levin, Phys. Rev. Lett. **57**, 877 (1986).
[23] S. Burdin, A. Georges, and D. R. Grempel, Phys. Rev. Lett. **85**, 1048 (2000).
[24] G.-M. Zhang and L. Yu, Phys. Rev. B **62**, 76 (2000).
[25] M. Lavagna and C. Pepin, Phys. Rev. B **62**, 6450 (2000).
[26] T. Senthil, M. Vojta, and S. Sachdev, Phys. Rev. B **69**, 035111 (2004).
[27] M. Vojta, Phys. Rev. B **78**, 125109 (2008).
[28] G.-M. Zhang, Y.-H. Su, and L. Yu, Phys. Rev. B **83**, 033102 (2011).
[29] J. Nilsson, Phys. Rev. B **83**, 235103 (2011).
[30] C. C. Yu and S. R. White, Phys. Rev. Lett. **71**, 3866 (1993).
[31] S. Moukouri and L. G. Caron, Phys. Rev. B. **52**, 15723(R) (1995).
[32] S. Moukouri and L. G. Caron, Phys. Rev. B. **54**, 12212 (1996).
[33] T. Mutou, N. Shibata, and K. Ueda, Phys. Rev. Lett. **81**, 4939 (1998).
[34] S. Smerat, U. Schollwock, I. P. McCulloch, and H. Schoeller, Phys. Rev. B **79**, 235107 (2009).
[35] F. F. Assaad, Phys. Rev. Lett. **83**, 796 (1999).
[36] Z.-P. Shi, R. R. P. Singh, M. P. Gelfand, and Z. Wang, Phys. Rev. B **51**, 15630(R) (1995).

[37] W. Zheng and J. Oitmaa, Phys. Rev. B **67**, 214406 (2003).
[38] H. Watanabe and M. Ogata, Phys. Rev. Lett. **99**, 136401 (2007).
[39] M. Z. Asadzadeh, F. Becca, and M. Fabrizio, Phys. Rev. B **87**, 205144 (2013).
[40] K. Kubo, J. Phys. Soc. Jpn. **84**, 094702 (2015).
[41] L. C. Martin and F. F. Assaad, Phys. Rev. Lett. **101**, 066404 (2008).
[42] L. C. Martin, M. Bercx, and F. F. Assaad, Phys. Rev. B **82**, 245105 (2010).
[43] R. Peters and N. Kawakami, Phys. Rev. B **92**, 075103 (2015).
[44] T. Sato, F. F. Assaad, and T. Grover, Phys. Rev. Lett. **120**, 107201 (2018).
[45] C. Jurecka and W. Brenig, Phys. Rev. B **64**, 092406 (2001).
[46] R. Eder, K. Grube, and P. Wróbel, Phys. Rev. B **93**, 165111 (2016).
[47] R. Eder and P. Wróbel, Phys. Rev. B **98**, 245125 (2018).
[48] R. Eder, Phys. Rev. B **99**, 085134 (2019).
[49] R. Eder, O. Stoica, and G. A. Sawatzky, Phys. Rev. B **55**, R6109 (1997).
[50] I. Martin and C. D. Batista, Phys. Rev. Lett. **101**, 156402 (2008).
[51] Y. Akagi and Y. Motome, J. Phys. Soc. Jpn. **79**, 083711 (2010).
[52] Y. Akagi and Y. Motome, J. Korean Phys. Soc. **63**, 405 (2012).
[53] Y. Motome, K. Nakamikawa, Y. Yamaji, and M. Udagawa, Phys. Rev. Lett. **105**, 036403 (2010).
[54] S. Hayami, M. Udagawa, and Y. Motome, J. Phys. Soc. Jpn. **80**, 073704 (2011).
[55] S. Hayami, M. Udagawa, and Y. Motome, J. Phys.: Conf. Ser. **400**, 032018 (2012).
[56] M. W. Aulbach, F. F. Assaad, and M. Potthoff, Phys. Rev. B **92**, 235131 (2015).
[57] S. Hayami, M. Udagawa, and Y. Motome, J. Phys. Soc. Jpn. **81**, 103707 (2012).
[58] K. Noda, T. Yoshida, R. Peters, and N. Kawakami, JPS Conf. Proc. **3**, 014019 (2014).
[59] H. Tsunetsugu, M. Sigrist, and K. Ueda, Rev. Mod. Phys. **69**, 809 (1997).
[60] B. H. Bernhard and C. Lacroix, Phys. Rev. B **92**, 094401 (2015).
[61] G.-B. Li, G.-M. Zhang, and L. Yu, Phys. Rev. B **81**, 094420 (2010).
[62] Y. Liu, G. M. Zhang, and L. Yu, Phys. Rev. B **87**, 134409 (2013).
[63] S. Süllow, M. C. Aronson, B. D. Rainford, and P. Haen, Phys. Rev. Lett. **82**, 2963 (1999).
[64] V. A. Sidorov, E. D. Bauer, N. A. Frederick, J. R. Jeffries, S. Nakatsuji, N. O. Moreno, J. D. Thompson, M. B. Maple, and Z. Fisk, Phys. Rev. B **67**, 224419 (2003).
[65] J. Larrea J., M. B. Fontes, A. D. Alvarenga, E. M. Baggio-Saitovitch, T. Burghardt, A. Eichler, and M. A. Continentino, Phys. Rev. B **72**, 035129 (2005).
[66] S. Drotziger, C. Pfleiderer, M. Uhlarz, H. v. Löhneysen, D. Souptel, W. Loser, and G. Behr, Phys. Rev. B **73**, 214413 (2006).